www.sciencemag.org/content/361/6400/392/suppl/DC1

Supplementary Materials for

The hippocampal engram maps experience but not place

Kazumasa Z. Tanaka*, Hongshen He, Anupratap Tomar, Kazue Niisato, Arthur J. Y. Huang, Thomas J. McHugh*

*Corresponding author. Email: kazumasa.tanaka@riken.jp (K.Z.T); thomas.mchugh@riken.jp (T.J.M)

Published 27 July 2018, *Science* **361**, 392 (2018)
DOI: 10.1126/science.aat5397

This PDF file includes:

Materials and Methods

Subject.

c-Fos-tTA mice (JAX 018306) were maintained on a C57BL/6J background by back-crossing for at least 5 generations. Eight animals were used for the main recordings and one was excluded because none of the tetrodes remained stable across all sessions. Two additional animals were used to estimate the background labeling in the home cage (see estimation of background labeling section below), two were used for examining the time course of ChR2 expression after seizure induction (FigS1), four were used to examine effects of OptID (FigS3), and another 20 animals were used for the contextual fear conditioning behavioral experiment (FigS8). All animals were provided with water and doxycycline containing food (40 mg/kg, Bioserv) *ad libitum,* and maintained in a temperature- and humidity-controlled room with a 12 h light/dark cycle (lights on from 08:00 A.M. to 8:00 P.M.). All experimental protocols were approved by the RIKEN Institutional Animal Care and Use Committee.

Virus vector and production.

For adeno-associated virus production, we used the AAV Helper Free System (Agilent Technologies). The adeno-associated virus vector, pAAV.TRE.hChR2(H134R).EYFP, was co-transfected with pAAV-DJ/8 (Cell Biolabs), which supplies AAV2 replication proteins and AAV-DJ/8 capsid proteins, and pHelper (Agilent Technologies) which supplies the necessary adenovirus gene products required for the AAV production into the 293FT cell line (Invitrogen) utilizing the 293fectin transfection reagent (Invitrogen). After 72 hours, the supernatant was collected and centrifuged at 3,000 rpm for 30 minutes and then filtered through a 0.45μM filtration unit (Millipore). Purification of the AAV was carried out by ultracentrifugation (87,000 g, 4ºC, 2 h) with a 20 % sucrose cushion. After ultracentrifugation, the supernatant was removed and the pellet was resuspended in phosphate-buffered saline (PBS), aliquoted and stored at -80˚C for long term storage. The titers for the AAV vectors used in this study ranged between 1.14 x 10^{12} to 1.06 x 10^{13} viral genome (vg)/mL.

Microdrive construction and surgery.

The microdrives consisted of 9 independently adjustable tetrodes (14 nm diameter, nichrome wire, gold plated to 200-300 k Ω) and 1 optic fiber (200 um diameter, Thorlabs, FT200EMT). These tetrodes were arranged to surround the optic fiber located in the center.

All animals were single-housed prior to surgery. During surgery, mice were anesthetized with avertin (2, 2, 2-tribromoethanol; Sigma-Aldrich, 476 mg/kg, i.p.) and 500 μL of AAV-TRE-hChR2(H134R)-EYFP vector was infused through a small craniotomy above the right dorsal CA1 (2.0 mm posterior, 1.5 mm lateral, and 1.3 mm ventral from the bregma) at a rate of 100 μL per minute with a micropump syringe (World Precision Instrument). After infusion, the 35G needle stayed at the infusion site for at least 15 minutes to allow diffusion of the vector. The microdrive was then implanted. The tip of the optic fiber was placed 2.0 mm posterior/1.5 mm lateral from the bregma and 1.0-1.2 mm ventral from the skull surface. One of stainless screws attached to the skull was used as an electrical ground for recording.

After surgery, animals were carefully monitored and i.p. injected with 0.5 mL of doxycycline solution (4 mg/mL in saline) when a loss of body weight (> 10%) was observed. In the 2-3 weeks after surgery the depth of the tetrodes were slowly and manually adjusted until stable recording of CA1 units was observed across days (see spike sorting section below). All

adjustments were conducted in a highly familiar small plastic red bucket (20 cm diameter) located in the recording room.
For the freezing experiment (Fig S8), animals were single housed and bilaterally infused with AAV-TRE- hChR2(H134R)-EYFP or AAV-TRE-EYFP (500 μL) to dorsal CA1 (2.0 mm posterior, ±1.5 mm lateral, and 1.3 mm ventral from the bregma). Optic fibers (200 um diameter, 1.4 mm length) were implanted at the same location. Black opaque dental cement was used to hold the fibers and to prevent light leakage from the skull.

Recording procedures.
Once stable recordings were achieved the mouse's doxycycline containing food was switched to normal food. During this OFF DOX period, mice remained in the familiar home cage without distraction or further adjustment of tetrodes to minimize background expression of the cFos-tTA transgene. Forty eight hours later the recording sessions were conducted. First, mice were exposed to a novel square chamber (30.5L x 24.1W x 21H cm, grid metal floor, ethanol odor, distinct visual cues on the walls, white noise) and allowed to explore for 30 minutes (context A; encoding). After this session, mice were brought back to the home cage and given doxycycline containing food (1 g/kg, Bioserve) to suppress further expression of ChR2. Twelve to fourteen hours later, they were exposed to the same chamber and again allowed to explore (context A; recall). Twenty four hours after the encoding session in A, an optogenetic identification session was recorded in the adjustment bucket. Finally, animals were exposed to a distinct square box (30.5L x 24.1W x 21H cm, flat plastic floor with beddings, banana odor, another set of distinct visual cues on the fluffy walls, baroque music) and allowed to explore for 30 minutes (context B; novel). Immediately before and after every exposure session, 30 minutes of rest sessions were recorded in the bucket to assess stability of spikes.
All data were acquired using 32-channel Digital Lynx 4SX acquisition system (Neuralynx). The local field potential (LFP) was filtered at 2-9000 Hz. Spike waveforms were filtered between 0.6-6 kHz and those above a peak threshold of 50 mV were time-stamped and digitized at 32,556 Hz. Light-emitting diodes (red and green) on the recording headstage were video tracked to obtain the animal's position and head direction.
All animals were transcardially perfused after recording sessions. Following post-fixation with 4% PFA (paraformaldehyde) solution, brains were sectioned (50 um thickness) and their ChR2 expression and tetrode locations marked by electrolytic lesions were confirmed.

Estimation of background labeling.
To estimate the percentage of cells labeled in the home cage prior to A (encoding) during the OFF DOX period, we recorded from two additional mice. These animals were taken OFF DOX for 48 hours, transported to the recording room, and stayed in the bucket for a mock rest recording sessions. After this procedure, they were brought back to the home cage with doxycycline containing food (1 g/kg). Twenty-four hours later, optogenetic identification session was recorded in the bucket. We observed light-induced spiking in 2 of 46 recorded neurons (4.35%) under these conditions.

Time course of ChR2 expression.
To determine the timing of ChR2 expression sufficient to produce spikes upon our OptID stimulation protocol we conducted a second control experiment. After 48 hours of OFF DOX, mice were i.p. injected with kainate acid (Sigma K0250; 20mg/kg in saline) to induce mild

seizure. This protocol is sufficient to induce c-Fos expression in virtually all CA1 pyramidal cells (*26*). After seizure onset, 15 minutes recording sessions with light stimulation through the optic fiber (473 nm, 10 mW, 0.5 Hz, 15 ms pulses) were conducted every two hours to determine when light induced population spikes were detected in CA1.

Effects of OptID

To examine effects of OptID on hippocampal physiology, we conducted two additional recording experiments using 4 mice (2 mice each). In the first experiment, animals were first OFF DOX labeled in a novel context A (30 min exploration). Three to five days later, they were allowed to explore a familiar context C (26L x 26W x 26H cm, black plastic floor, acetic acid odor, black plastic walls). Immediately after this session, the recording area was laser stimulated with the same parameters used for OptID in the main experiment (0.5 Hz, 15 ms pulses, 10 mW, 30 min), followed by another exploration in the context C. In the second experiment, animals were laser stimulated (OptID1: 0.5 Hz, 15 ms pulses, 10 mW, 30 min) and then allowed to explore a novel context D for 30 min (30.5L x 24.1W x 21H cm, floor covered with a Kim towel, almond odor, metal walls, fan noise). Then they were taken OFF DOX for 5 days and stayed in their home cage to randomly label CA1 pyramidal cells. After returning the mice to ON DOX conditions, the same animals were again laser stimulated (OptID2: 0.5 Hz, 15 ms pulses, 10 mW, 30 min) and then allowed to explore another novel context E (42L x 40W x 33H cm, rubber floor, ethanol odor, black walls).

Spike sorting.

Spikes were manually sorted using SpikeSort3D software (Neuralynx) as previously described (*27*). In short, waveform amplitudes of all spikes recorded from three channels were projected to three dimensional space and putative units were clustered. This procedure was repeated for all combinations of channels and also for energy of spikes.

For each exposure session, spikes from pre-exposure rest sessions were also examined and clusters with > 0.5% spikes having inter-spike-interval of < 2 ms, a total # of spikes < 50, or an isolation distance < 10 in the rest session were excluded.

Clustered units were matched across sessions as previously described (*28*). Briefly, units that passed our criteria across sessions were considered to be the same only when a small adjustment of boundaries was sufficient to match the clusters (Fig. S4A). Furthermore, two experimenters (KZT and TJM) independently conducted spike sorting and cluster matching, and obtained concurrent results. Through cluster matching and optogenetic identification (see below), we excluded 268 units and accepted 148 CA1 cells for further analysis (416 cells in total).

All analyses described below (except for statistical tests) were performed using scripts written in MATLAB (MathWorks).

Optogenetic identification.

Prior to the optogenetic identification session, the optic fiber in the microdrive was coupled to 473 nm DPSS laser (Shanghai Laser & Optics Century, BL473T8-300FC). During the 30 minutes session blue light (10 mW, 0.5 Hz, 15 ms pulses) was delivered to the CA1 while recording spikes and LFP. Cells with average firing rate increases during the 15 ms light epochs greater than 5 standard deviations (SD) above baseline were considered to be light-responsive and thus c-Fos positive. If all clustered units and the unclustered spikes from a tetrode were not light-responsive, data from this tetrode were discarded as we were unable to determine whether

1) all units were c-Fos negative or 2) light did not reach this tetrode. Across all mice 29 of 148 stably recorded CA1 pyramidal cells met these criteria and were labeled as c-Fos positive. To determine if we can attribute differences between c-Fos positive and negative cells to differences in cluster quality, we compared isolation distance and L-ratio between these two populations of cells across sessions and found no significant differences (Fig. S4B).

Place fields.

Animal's trajectories were corrected by removing artifacts caused by transient tracking errors and were smoothed with a Gaussian kernel of 0.05 SD width. Firing rate maps were obtained as follows. First, spikes from each cell were assigned to 1 cm x 1 cm spatial bins. Then the number of spikes for each bin was divided by the occupancy time of that bin. Finally, they were smoothed with a 1 SD Gaussian kernel. For visualization purpose, images in the main figures were further smoothed with 7 spatial bins.

In order to avoid bias we applied a loose criteria for place cells. Cells having a Complex Spike Index (CSI) greater than 5 and a mean firing rate higher than 1 Hz were considered to be pyramidal cells. CSI was defined as previously described (*6*). Mean firing rates were calculated by averaging the firing rate of each unit when the velocity of the mouse exceeded 2 cm/sec. Peak firing rates were defined as rate in the spatial bin having the maximal value. Place field size was calculating by summing the number of spatial bins where a neuron's firing rate exceed 20% of its peak rate. Spatial information was calculated as previously described (*29*). Cells having mean firing rates higher than 10 Hz and place field sizes bigger than 1/3 of the entire area were considered to be interneurons and excluded from analysis.

Spatial correlations were calculated as the Pearson's correlation coefficient between 2 firing rate maps of place cells that were active in both sessions (*30*). In Figure 4C, firing rate correlations refer to absolute values of differences of mean firing rates divided by their sum. In Figure 4H and J, we calculated population correlations of mean firing rates from subsets of recorded cells. First, based on our results from OptID recordings in home cage animals we estimated 4.35% of all cells recorded were labeled in the home cage during OFF DOX. Thus, from the c-Fos positive population, these background cells were randomly selected and discarded from further analysis. A Pearson's correlation coefficient of population vectors consisted of mean firing rates of the remaining positive cells from the two sessions was defined as a population correlation measure. The same number of c-Fos negative cells was also randomly subsampled and the population correlations were calculated. We repeated this process 1,000 times to estimate distributions of this measure depending on cell identities discarded. The discrimination index was defined as difference of the population correlations from c-Fos positive and negative cells divided by their sum.

Burst analysis.

A burst was defined as 2 or more spikes occurring with an inter-spike-interval between 3 (refractory period) and 15 msec. Theta modulation index of burst activity was calculated as a burst auto-correlation within theta range (6-12 Hz). An auto-correlogram of burst spike rates (10 msec bin) were generated to obtain burst rates within theta range (inter-burst-interval of 83.3 – 166.7 msec) and baseline burst rates (those outside of the range). Absolute differences of burst rates for each bin (theta bursts – baseline bursts) were summed to estimate degree of theta modulation of burst activity. As an additional measure for this theta modulation, we also

calculated power spectrums of burst trains (*31*). The burst auto-correlations were Fourier transformed and power of frequency content was examined.

LFP analysis.

The raw local field potential (LFP) data were down-sampled using custom software written in C to 1627.8 Hz (a factor of 20), followed by quality control measures which excluded any signals that were either saturated or had a signal (4-12 Hz) to noise (45-55 Hz) ratio > 6dB. A low-pass filter with a cut-off frequency equal to half the target sampling frequency was applied to the LFP prior to down-sampling to prevent signal distortion.

To examine the relation of spikes to the theta oscillation, we selected the LFP channel having the highest power of theta among tetrodes in each animal. Theta band signals were obtained by band-pass filtering these LFP traces. Hilbert transformation with interpolation was applied to estimate instantaneous theta phase (0 degree is peak and 180 is trough). Each spike was assigned to a theta phase (10 degree bins) to calculate firing probability for each theta phase. In Fig. 3, A and B, only cells significantly phase locked to theta ($p < 0.05$, Rayleigh test) were plotted.

To examine the spike-gamma relations, we used the LFP recorded on the same channel used for unit spike detection. We detected gamma events as previously described (*32*). 30-50 Hz and 55-85 Hz frequency bands were used as slow and fast gamma (*33*).Instantaneous gamma phase was calculated in the same way as theta. Cells phase locked to either gamma event had phase distribution significantly different from uniform distribution ($p < 0.05$, Rayleigh test).

Freezing experiment.

We conducted the freezing experiment with optogenetic engram activation (FigS8) as previously described (*24*). Briefly, two weeks after the surgery, animals were handled by an experimenter for 3 successive days (1-2 min per day). After handling, they were first habituated in context A (30.5L x 24.1W x 21H cm, white plastic floor, almond odor, red room light) with laser stimulation (473 nm, 4 Hz, 15 ms pulses, 10 mW). This habituation session was 12 min in duration (alternating 3 min light off and 3 min light on epochs). After this habituation, mice were taken OFF DOX for 24-30 hours, followed by a contextual fear conditioning session in context B (30.5L x 24.1W x 21H cm, metal grid floor, acetic acid odor, triangle ceiling). This training session was 330 sec in duration. At 150, 210, 270 sec, mice received a 2 second foot shock (0.75 mA) through the grid floor. After the training, mice were switched back to ON DOX food (40 mg/kg). Twenty four hours after training, mice were tested in context B without foot shocks (180 sec in duration). Finally, mice were tested in context A for 5 days. These testing sessions were identical to the habituation session. An experimenter (KZT), who was blind to the groups, scored freezing behavior. In Fig. S8D, freezing rates averaged over 5 testing sessions were plotted.

All animals were transcardially perfused after the freezing experiment. Following post-fixation with 4% PFA (paraformaldehyde) solution, brains were sectioned (50 um thickness) and ChR2/EYFP expression and fiber locations were confirmed.

Statistical tests.

All statistical tests were performed using R. Wilcoxon rank sum or signed rank test was used for group/pair-wise comparisons. Where appropriate, two-way ANOVA was conducted, and if needed, followed by pair-wise post-hoc non-parametric rank sum comparisons with p-value correction in a Bonferroni manner (divided by the number of comparisons). For statistical tests of circular data, Watson-Wheeler test was performed to test homogeneity of means. P-values for

comparing subsampled data correlations were calculated as probabilities of observing values expected when the null hypothesis is true. For example, in Fig. 4G, this refers to a probability to observe a higher ensemble correlation in context A/B than context A/A. All values reported in the text are written as mean ± SEM.

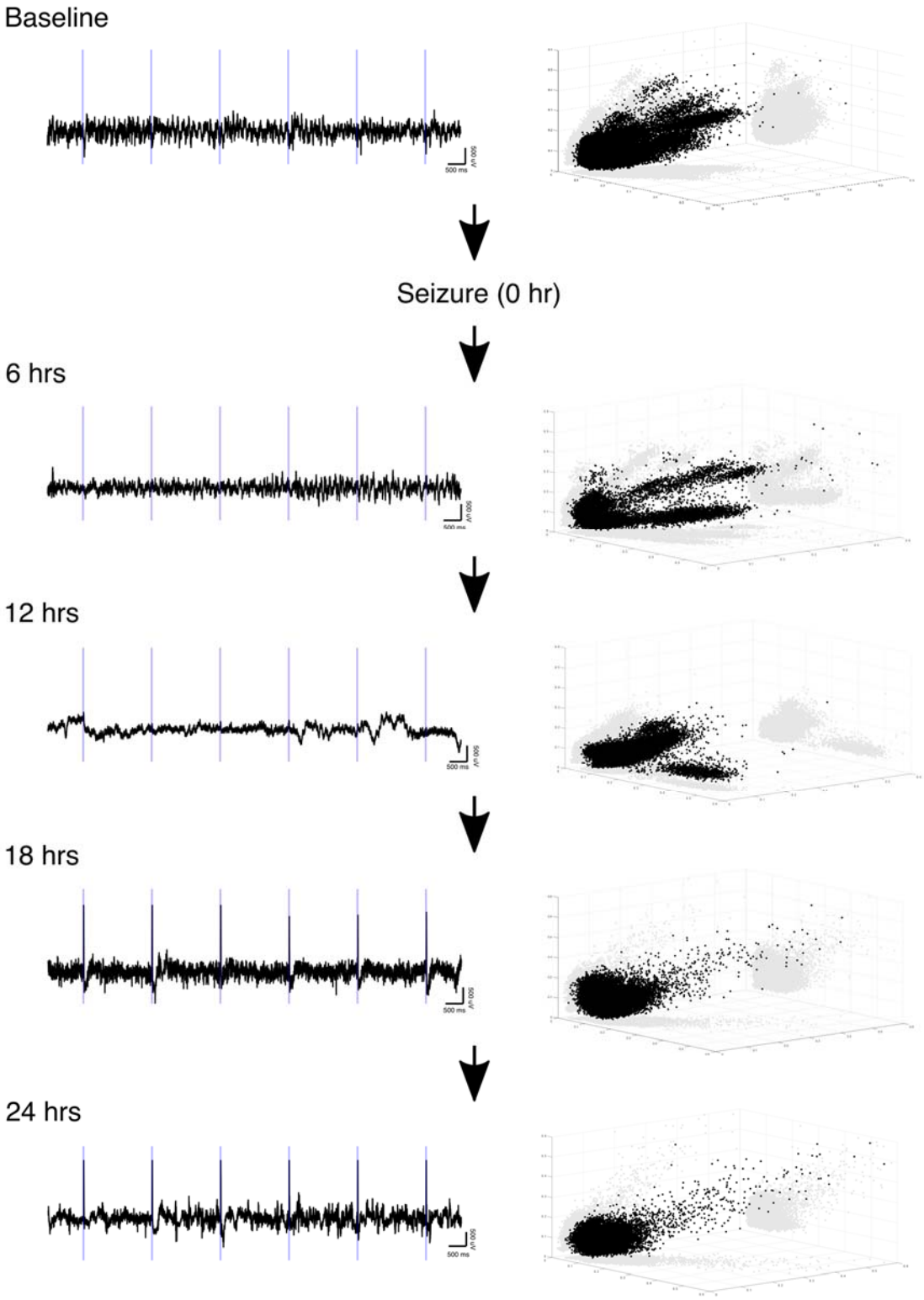

Fig. S1.

Time course of ChR2 expression under c-Fos-tTA system. Raw LFP traces (top) and three-dimensional projections of spikes (bottom; peak amplitudes of spike wave forms simultaneously

detected from three channels are used) during light stimulation sessions are plotted. From left, baseline stimulation session (OFF DOX, before seizure induction), 6, 12, 18, 24 hours after seizure onset. Epileptic seizure was no longer observed in these time points.

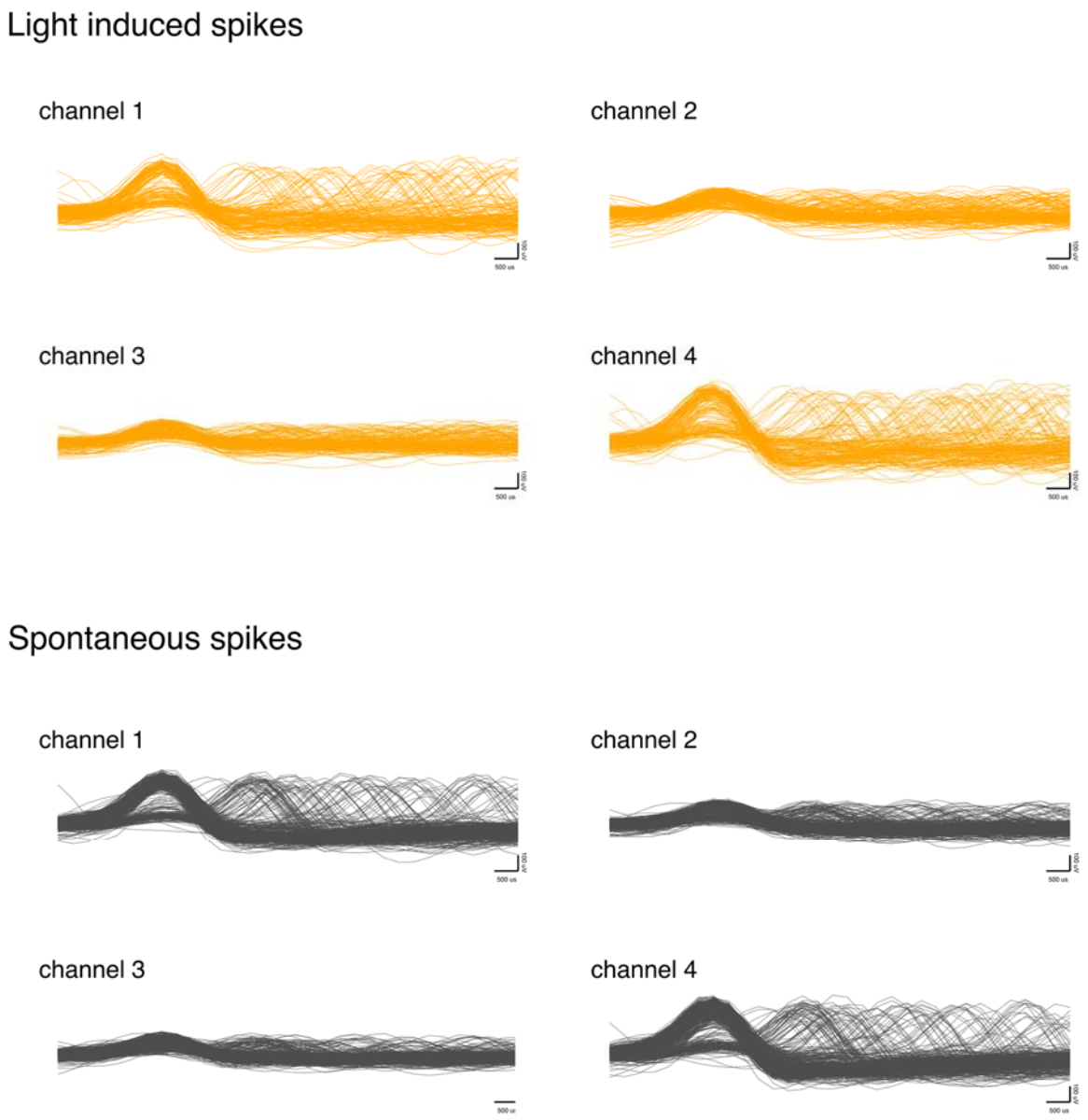

Fig. S2.

Spike wave-forms of spontaneous (black) or light-induced spikes (orange) during the OptID session. Wave forms of simultaneously detected from all four channels are plotted.

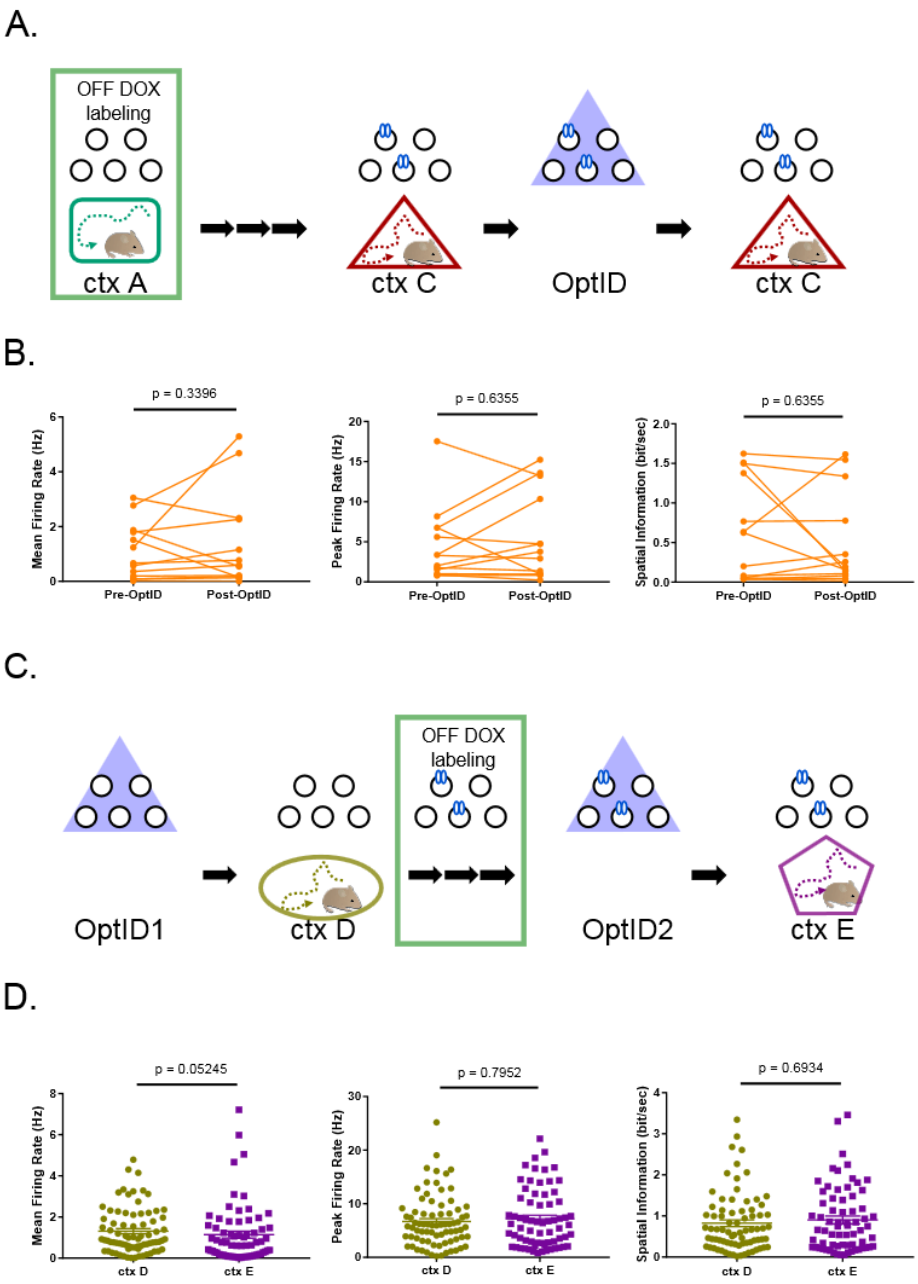

FigureS3.
Effects of OptID on hippocampal physiology. **A.** Experimental design to examine effects of OptID on spatial representation of a familiar context C. Animals were first OFF DOX labeled in a novel context A. Three to five days later, they were allowed to explore a familiar context C. Immediately after this session, the recording area was laser stimulated with the same parameters used for OptID in the main experiment (0.5 Hz, 15 ms pulses, 10 mW, 30 min), followed by another exploration in the context C. This OptID session identified 31.71% of recorded cells (n = 13) as being labeled in Ctx A. **B.** Comparisons of mean, peak firing rates, or spatial information of labeled CA1 cells between pre- and post-OptID session. Wilcoxon matched pairs signed rank

test revealed no significant effect in any measures (mean firing rate, pre 1.097 ± 0.2878 vs post 1.409 ± 0.4891 Hz, W = 29, p = 0.3396; peak firing rate, pre 4.577 ± 1.288 vs post 5.617 ± 1.523 Hz, W = 15, p = 0.6355; spatial information, pre 0.6541 ± 0.178 vs post 0.5101 ± 0.1661 Hz, W = -15, p = 0.6355). **C.** Experimental design to examine effects of OptID on spatial map formation in novel contexts D/E. First, animals were laser stimulated (OptID1: 0.5 Hz, 15 ms pulses, 10 mW, 30 min) and then allowed to explore a novel context D. Then they were taken off DOX for a prolonged duration to randomly label CA1 cells. After putting back to ON DOX, the same animals were again laser stimulated (OptID2: 0.5 Hz, 15 ms pulses, 10 mW, 30 min) and then allowed to explore another novel context E. No cell showed light-induced spikes during OptID1, and 43.3% of cells showed light-induced spikes during OptID2. **D.** Comparisons of mean, peak firing rates, or spatial information (bit/sec) of CA1 cells between pre- and post-OptID session (cells are not matched). Wilcoxon rank sum tests revealed no significant effect in any measures (n = 77 for ctx D, n = 68 for ctx E; mean firing rate, ctx D 1.309 ± 0.126 vs ctx E 1.14 ± 0.1721 Hz, W = 3108, p = 0.05245; peak firing rate, ctx D 6.68 ± 0.5517 vs ctx E 7.193 ± 0.6574 Hz, W = 2552, p = 0.7952; spatial information, ctx D 0.8235 ± 0.0819 vs ctx E 0.9042 ± 0.09476 Hz, W = 2518, p = 0.6934).

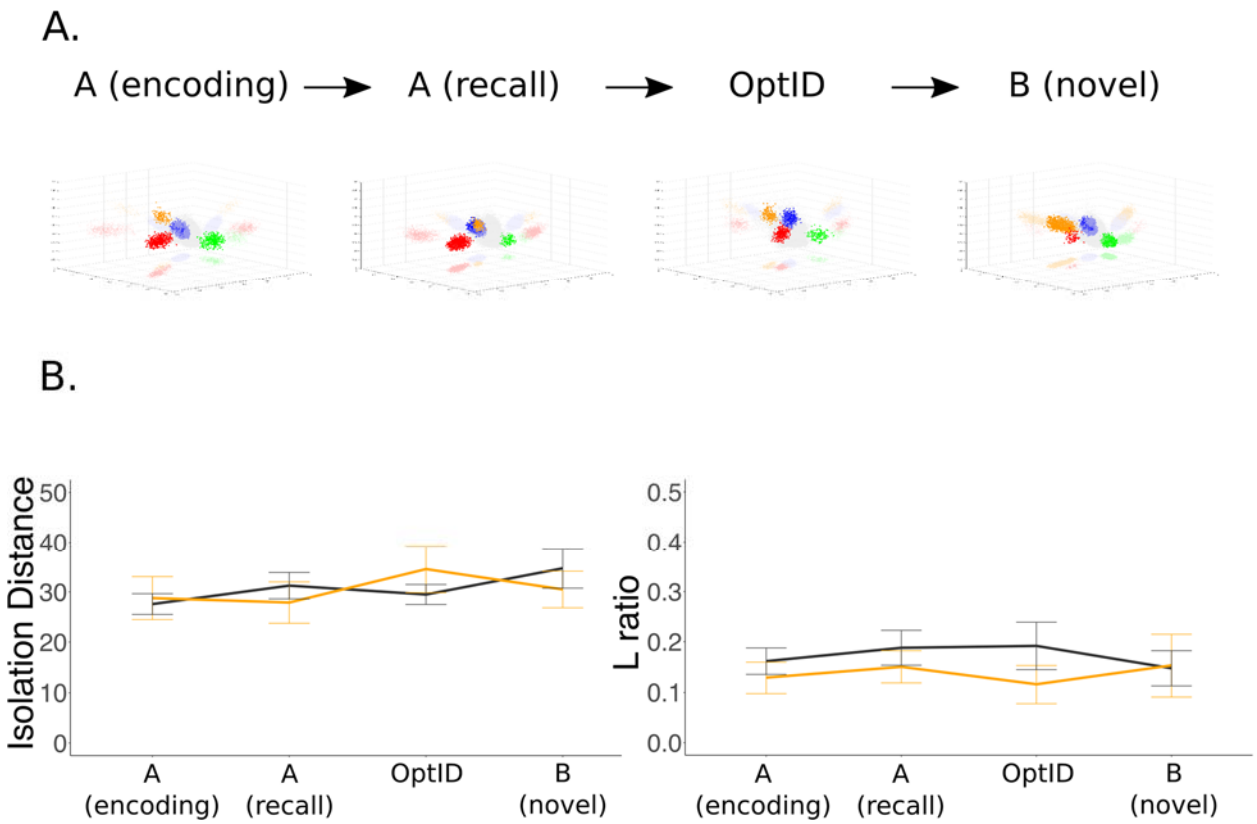

Fig. S4.

Units stably tracked across sessions. **A.** Three-dimensional projections of spikes (peak amplitudes of spike wave forms simultaneously detected from three channels are used; matched units are color-coded) from a stable tetrode across four recording sessions. **B.** Unit qualities (isolation distance and L ratio) across sessions (mean ± SEM). Two-way repeated ANOVA revealed no significant difference between cell types across sessions (isolation distance, , no significant effect by interaction ($F_{(3,363)} = 0.24$, $p = 0.87$), cell type ($F_{(1, 121)} = 1.21$, $p = 0.27$), or session ($F_{(3, 363)} = 0.62$, $p = 0.60$); L ratio, no significant effect by interaction ($F_{(3,363)} = 0.36$, $p = 0.78$), cell type ($F_{(1, 121)} = 0.19$, $p = 0.67$), or session ($F_{(3, 363)} = 1.098$, $p = 0.35$).

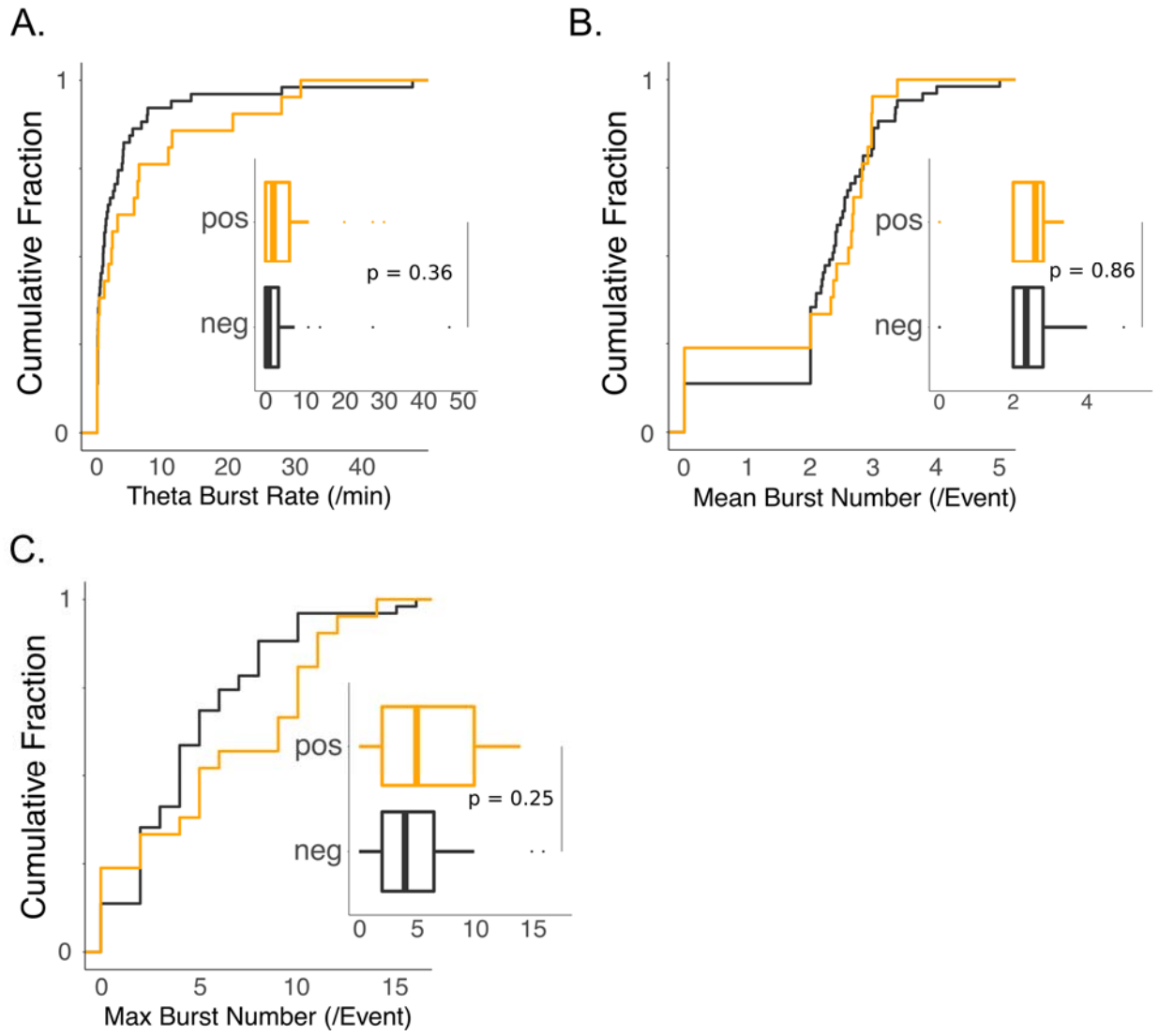

Fig. S5.

Theta burst events in c-Fos positive cells and negative cells when animals explore a distinct context B. Cumulative density plots and boxplots comparing **A.** TBE rates (A, pos 6.11 ± 1.99 vs neg 3.48 ± 1.10 theta bursts/min, W = 462, p = 0.36), **B.** mean burst number per TBE (pos 2.66 ± 0.081 vs neg 2.58 ± 0.089 bursts per TBE, W = 520.5, p = 0.86), and **C.** maximum burst number within a single TBE (pos 7.81 ± 0.80 vs neg 5.34 ± 0.47 bursts in the longest TBE, W = 442, p = 0.25) of the two cell types.

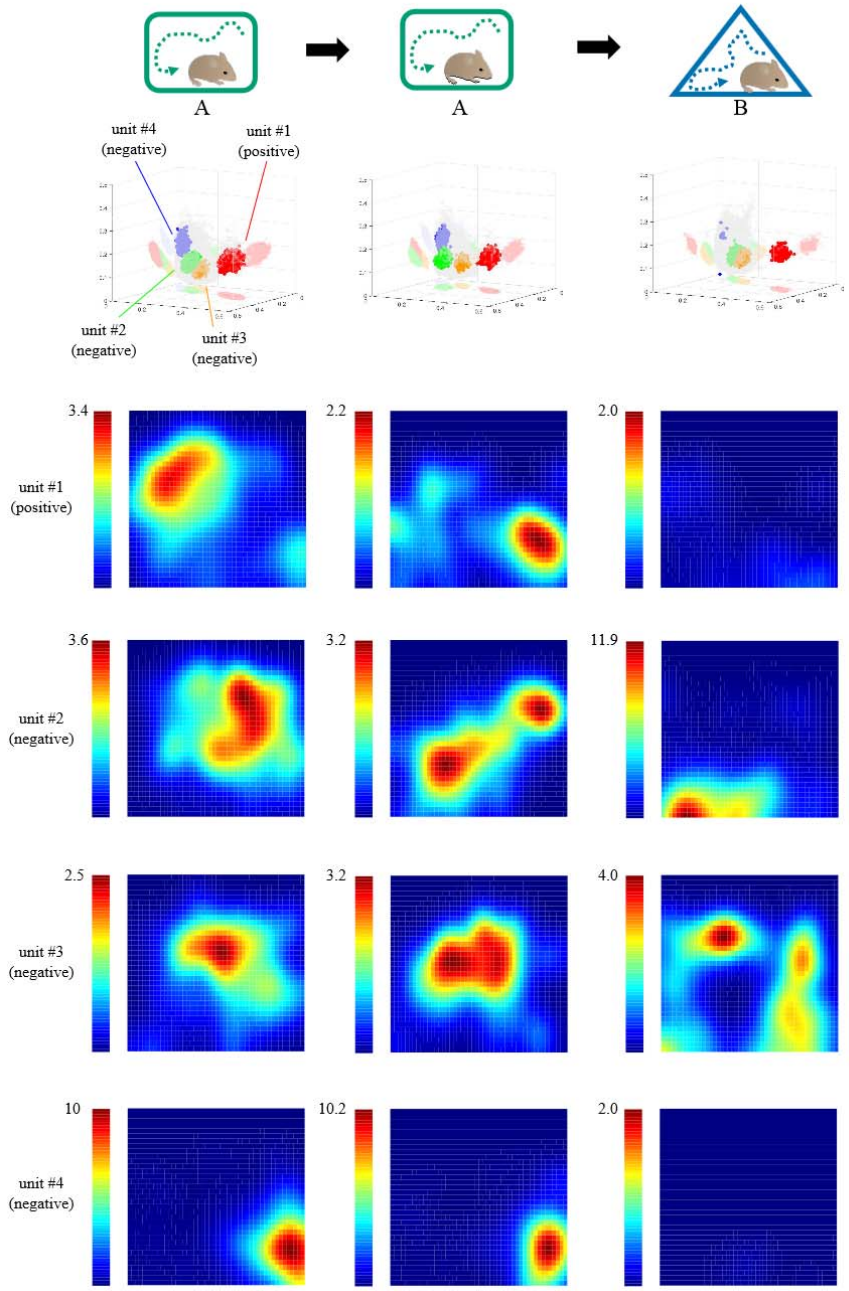

FigureS6.
Examples of stable recording of c-Fos positive/negative place cells across three sessions. Top, schematics of the recording procedure. As described in the main text, OptID session was conducted between the second context A exploration and context B. Middle, three-dimensional projections of spikes (peak amplitudes of spike wave forms simultaneously detected from three channels are used; matched units are color-coded) from a stable tetrode across all recording sessions. Bottom, firing rate maps of each unit for each session. Color scale bars represent firing rate (Hz).

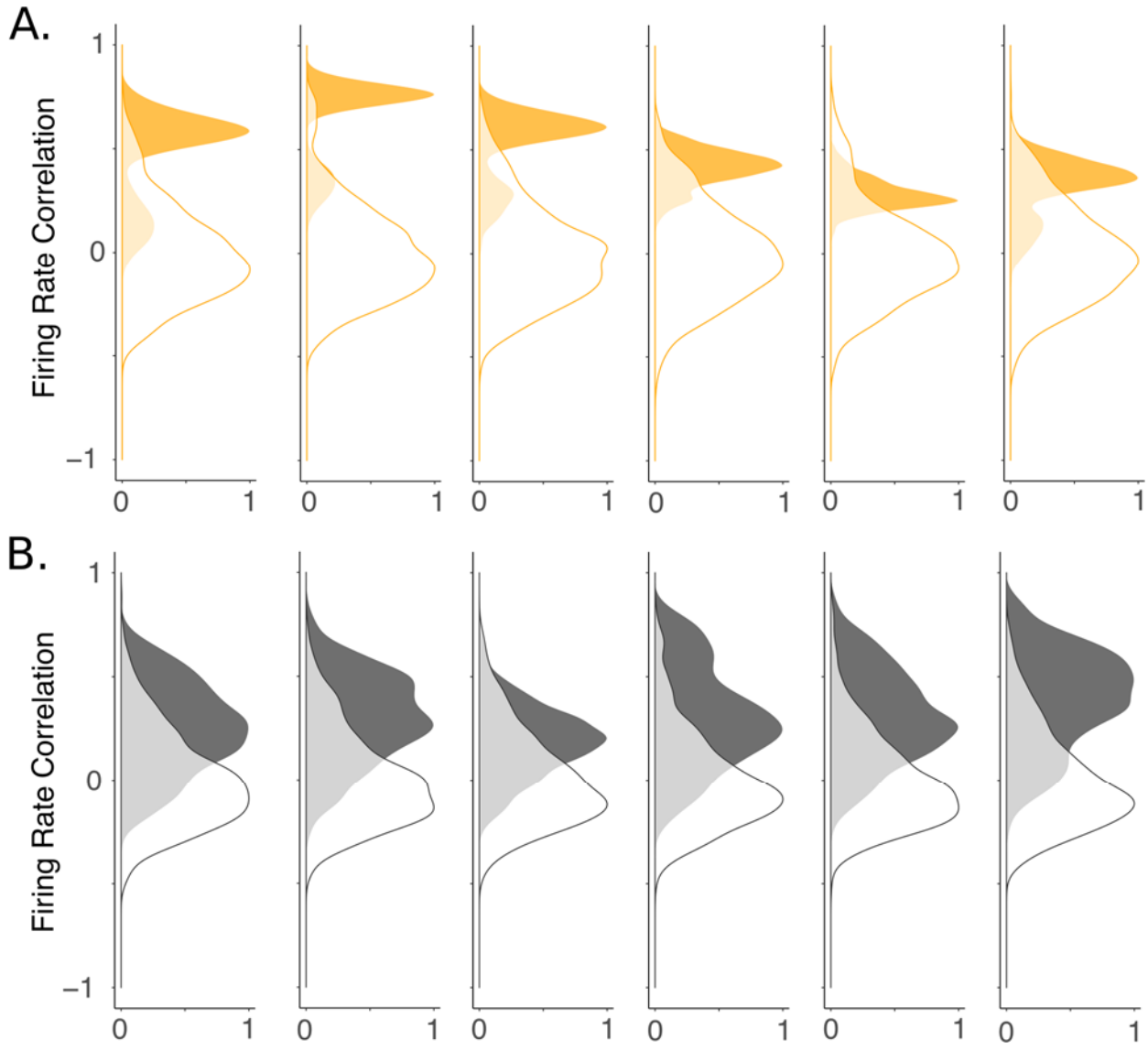

Fig S7.

Instantaneous ensemble firing rate correlation, comparing subsampled original data and shuffled data recorded during the initial 6 minutes of recall in Context A in 1 min bins. A cell ensemble was subsampled from pos or neg population as in Fig. 4. For the shuffled data, cell IDs from each subsample were shuffled to create mismatch between sessions and calculated Pearson correlations of the firing rate vectors during A (encoding) and 1 min bin of A (recall). This value was compared to the firing rate correlation obtained from the original data, and a p-value was reported as a probability to find a higher correlation in the shuffled data. (**A**) Probability to find a higher correlation in shuffled positive data than original positive data, p = 0.004, 0, 0, 0, 0.01 for 1-6 min bins, p = 0.002 for the first 10 sec bin. (**B**) Probability to find a higher correlation in shuffled negative data than original negative data, p = 0.13, 0.102, 0.144, 0.103, 0.068, 0.058 for 1-6 min bins, p = 0.251 for the first 10 sec bin

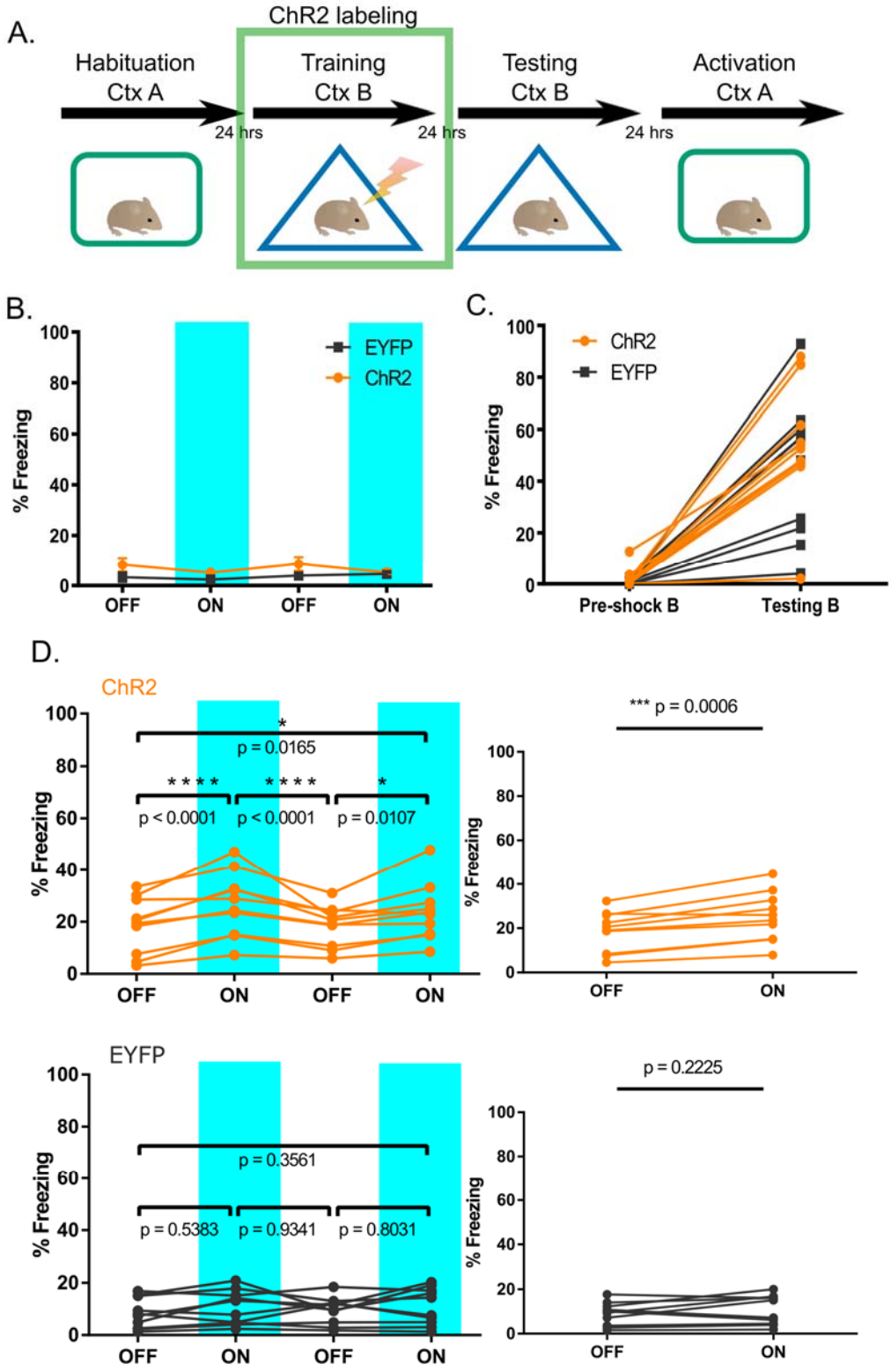
A.
ChR2 labeling
Habituation
Ctx A
Training
Ctx B
Testing
Ctx B
Activation
Ctx A
24 hrs
24 hrs
24 hrs
B.
% Freezing
EYFP
ChR2
OFF
ON
OFF
ON
C.
% Freezing
ChR2
EYFP
Pre-shock B
Testing B
D.
ChR2
% Freezing
*
p = 0.0165
****
p < 0.0001
****
p < 0.0001
*
p = 0.0107
OFF
ON
OFF
ON
*** p = 0.0006
OFF
ON
EYFP
p = 0.3561
p = 0.5383
p = 0.9341
p = 0.8031
p = 0.2225

FigureS8.
Optogenetic activation of CA1 engram formed during contextual fear conditioning. **A.** Experimental design. After habituation to context A and laser stimulation (4 Hz, 15 ms, 10 mW), mice were taken OFF DOX for 24 to 30 hrs before contextual fear conditioning in context B and then immediately returned to the ON DOX condition. Mice were first tested once in context B with no stimulation to assess fear acquisition, then tested in context A with laser stimulation daily for 5 days. N = 10 for ChR2, N = 10 for EYFP. **B.** Percent freezing during habituation in context A. Laser stimulation did not induce freezing behavior in the unlabeled mice (Two-way repeated ANOVA, no significant effect of epoch, $F_{(3,54)} = 1.633$, $p = 0.1925$). **C.** Percent freezing in context B during a pre-shock epoch on the training day and during testing next day. Significant increase in percent freezing indicates a robust association between context B and foot shocks (Two-way repeated ANOVA, a significant main effect of session, $F_{(1,18)} = 70.91$, $p < 0.0001$). **D.** Percent freezing in context A during laser ON/OFF epochs (top: ChR2, bottom: EYFP). Two-way repeated ANOVA revealed a significant interaction effect (epoch x genotype, $F_{(3,54)} = 3.694$, $p = 0.0172$). Post-hoc comparisons between laser ON vs OFF epochs found significant differences in ChR2 animals but not in EYFP animals (p-values are Bonferroni corrected). Right panels, percent freezing in context A, scores from two laser epochs are averaged. Pair-wise t-tests found significant difference in ChR2 animals, but again not in EYFP animals.

References and Notes

1. M. L. Shapiro, H. Eichenbaum, Hippocampus as a memory map: Synaptic plasticity and memory encoding by hippocampal neurons. *Hippocampus* **9**, 365–384 (1999). doi:10.1002/(SICI)1098-1063(1999)9:4<365:AID-HIPO4>3.0.CO;2-T Medline

2. G. Buzsáki, E. I. Moser, Memory, navigation and theta rhythm in the hippocampal-entorhinal system. *Nat. Neurosci.* **16**, 130–138 (2013). doi:10.1038/nn.3304 Medline

3. J. O'Keefe, L. Nadel, *The Hippocampus as a Cognitive Map* (Oxford Univ. Press, 1978).

4. O. Jensen, J. E. Lisman, Position reconstruction from an ensemble of hippocampal place cells: Contribution of theta phase coding. *J. Neurophysiol.* **83**, 2602–2609 (2000). doi:10.1152/jn.2000.83.5.2602 Medline

5. C. Kentros, E. Hargreaves, R. D. Hawkins, E. R. Kandel, M. Shapiro, R. V. Muller, Abolition of long-term stability of new hippocampal place cell maps by NMDA receptor blockade. *Science* **280**, 2121–2126 (1998). doi:10.1126/science.280.5372.2121 Medline

6. T. J. McHugh, K. I. Blum, J. Z. Tsien, S. Tonegawa, M. A. Wilson, Impaired hippocampal representation of space in CA1-specific NMDAR1 knockout mice. *Cell* **87**, 1339–1349 (1996). doi:10.1016/S0092-8674(00)81828-0 Medline

7. T. J. Teyler, P. DiScenna, The hippocampal memory indexing theory. *Behav. Neurosci.* **100**, 147–154 (1986). doi:10.1037/0735-7044.100.2.147 Medline

8. T. J. Teyler, J. W. Rudy, The hippocampal indexing theory and episodic memory: Updating the index. *Hippocampus* **17**, 1158–1169 (2007). doi:10.1002/hipo.20350 Medline

9. R. M. Grieves, K. J. Jeffery, The representation of space in the brain. *Behav. Processes* **135**, 113–131 (2017). doi:10.1016/j.beproc.2016.12.012 Medline

10. J. J. Kim, M. S. Fanselow, Modality-specific retrograde amnesia of fear. *Science* **256**, 675–677 (1992). doi:10.1126/science.1585183 Medline

11. J. W. Rudy, R. C. O'Reilly, Conjunctive representations, the hippocampus, and contextual fear conditioning. *Cogn. Affect. Behav. Neurosci.* **1**, 66–82 (2001). doi:10.3758/CABN.1.1.66 Medline

12. J. F. Guzowski, B. L. McNaughton, C. A. Barnes, P. F. Worley, Environment-specific expression of the immediate-early gene Arc in hippocampal neuronal ensembles. *Nat. Neurosci.* **2**, 1120–1124 (1999). doi:10.1038/16046 Medline

13. M. VanElzakker, R. D. Fevurly, T. Breindel, R. L. Spencer, Environmental novelty is associated with a selective increase in Fos expression in the output elements of the hippocampal formation and the perirhinal cortex. *Learn. Mem.* **15**, 899–908 (2008). doi:10.1101/lm.1196508 Medline

14. L. G. Reijmers, B. L. Perkins, N. Matsuo, M. Mayford, Localization of a stable neural correlate of associative memory. *Science* **317**, 1230–1233 (2007). doi:10.1126/science.1143839 Medline

15. S. Tonegawa, X. Liu, S. Ramirez, R. Redondo, Memory engram cells have come of age. *Neuron* **87**, 918–931 (2015). doi:10.1016/j.neuron.2015.08.002 Medline

16. S. A. Josselyn, S. Köhler, P. W. Frankland, Finding the engram. *Nat. Rev. Neurosci.* **16**, 521–534 (2015). doi:10.1038/nrn4000 Medline

17. K. K. Tayler, K. Z. Tanaka, L. G. Reijmers, B. J. Wiltgen, Reactivation of neural ensembles during the retrieval of recent and remote memory. *Curr. Biol.* **23**, 99–106 (2013). doi:10.1016/j.cub.2012.11.019 Medline

18. Local field potential and single-unit spiking were recorded during every session, as well as during pre- and postexposure rest to ensure recording stability (fig. S4).

19. L. L. Colgin, T. Denninger, M. Fyhn, T. Hafting, T. Bonnevie, O. Jensen, M. B. Moser, E. I. Moser, Frequency of gamma oscillations routes flow of information in the hippocampus. *Nature* **462**, 353–357 (2009). doi:10.1038/nature08573 Medline

20. E. Edelmann, E. Cepeda-Prado, M. Franck, P. Lichtenecker, T. Brigadski, V. Leßmann, Theta Burst Firing Recruits BDNF Release and Signaling in Postsynaptic CA1 Neurons in Spike-Timing-Dependent LTP. *Neuron* **86**, 1041–1054 (2015). doi:10.1016/j.neuron.2015.04.007 Medline

21. B. Kuzniewska, E. Rejmak, A. R. Malik, J. Jaworski, L. Kaczmarek, K. Kalita, Brain-derived neurotrophic factor induces matrix metalloproteinase 9 expression in neurons via the serum response factor/c-Fos pathway. *Mol. Cell. Biol.* **33**, 2149–2162 (2013). doi:10.1128/MCB.00008-13 Medline

22. E. Amin, J. M. Pearce, M. W. Brown, J. P. Aggleton, Novel temporal configurations of stimuli produce discrete changes in immediate-early gene expression in the rat hippocampus. *Eur. J. Neurosci.* **24**, 2611–2621 (2006). doi:10.1111/j.1460-9568.2006.05131.x Medline

23. T. Otto, H. Eichenbaum, S. I. Wiener, C. G. Wible, Learning-related patterns of CA1 spike trains parallel stimulation parameters optimal for inducing hippocampal long-term potentiation. *Hippocampus* **1**, 181–192 (1991). doi:10.1002/hipo.450010206 Medline

24. T. J. Ryan, D. S. Roy, M. Pignatelli, A. Arons, S. Tonegawa, Engram cells retain memory under retrograde amnesia. *Science* **348**, 1007–1013 (2015). doi:10.1126/science.aaa5542 Medline

25. K. Z. Tanaka, A. Pevzner, A. B. Hamidi, Y. Nakazawa, J. Graham, B. J. Wiltgen, Cortical representations are reinstated by the hippocampus during memory retrieval. *Neuron* **84**, 347–354 (2014). doi:10.1016/j.neuron.2014.09.037 Medline

26. L. M. Yu, D. Polygalov, M. E. Wintzer, M.-C. Chiang, T. J. McHugh, CA3 Synaptic Silencing Attenuates Kainic Acid-Induced Seizures and Hippocampal Network Oscillations. *eNeuro* **3**, ENEURO.0003-16.2016 (2016). doi:10.1523/ENEURO.0003-16.2016 Medline

27. R. Boehringer, D. Polygalov, A. J. Y. Huang, S. J. Middleton, V. Robert, M. E. Wintzer, R. A. Piskorowski, V. Chevaleyre, T. J. McHugh, Chronic loss of CA2 transmission leads to hippocampal hyperexcitability. *Neuron* **94**, p642–655.e9 (2017). doi:10.1016/j.neuron.2017.04.014 Medline

28. E. A. Mankin, F. T. Sparks, B. Slayyeh, R. J. Sutherland, S. Leutgeb, J. K. Leutgeb, Neuronal code for extended time in the hippocampus. *Proc. Natl. Acad. Sci. U.S.A.* **109**, 19462–19467 (2012). doi:10.1073/pnas.1214107109 Medline

29. W. E. Skaggs, B. L. McNaughton, K. M. Gothard, E. J. Markus, An information-theoretic approach to deciphering the hippocampal code, in *Advances in Neural Processing Systems* 5, S. J. Hanson, C. L. Giles, J. D. Cowan, Eds. (Morgan Kaufmann, 1993), pp. 1030–1037.

30. J. K. Leutgeb, S. Leutgeb, M.-B. Moser, E. I. Moser, Pattern separation in the dentate gyrus and CA3 of the hippocampus. *Science* **315**, 961–966 (2007). doi:10.1126/science.1135801 Medline

31. C. Koch, I. Segev, *Methods in Neuronal Modeling* (MIT Press, 1998).

32. K. Mizuseki, K. Diba, E. Pastalkova, G. Buzsáki, Hippocampal CA1 pyramidal cells form functionally distinct sublayers. *Nat. Neurosci.* **14**, 1174–1181 (2011). doi:10.1038/nn.2894 Medline

33. S. J. Middleton, T. J. McHugh, Silencing CA3 disrupts temporal coding in the CA1 ensemble. *Nat. Neurosci.* **19**, 945–951 (2016). doi:10.1038/nn.4311 Medline